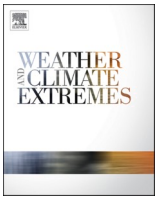
Weather and Climate Extremes 40 (2023) 100561



Contents lists available at ScienceDirect

Weather and Climate Extremes

journal homepage: www.elsevier.com/locate/wace





# Hysteresis and irreversibility of global extreme precipitation to anthropogenic $CO_2$ emission

Sanjit Kumar Mondal [a], Soon-Il An [a,b,c,*], Seung-Ki Min [c,d], Soong-Ki Kim [a], Jongsoo Shin [c], Seungmok Paik [a], Nari Im [a], Chao Liu [a]

[a] Irreversible Climate Change Research Center, Yonsei University, Seoul, South Korea
[b] Department of Atmospheric Sciences, Yonsei University, Seoul, South Korea
[c] Division of Environmental Science and Engineering, Pohang University of Science and Technology, Pohang, South Korea
[d] Institute for Convergence Research and Education in Advanced Technology, Yonsei University, Incheon, South Korea

ARTICLE INFO

*Keywords:*
Climate change
Extreme precipitation
Hysteresis
Reversibility
Carbon dioxide removal
Population exposure

ABSTRACT

Understanding of extreme precipitation change in response to $CO_2$ forcing and associated socioeconomic exposure is limited. In this study, a comprehensive analysis is conducted to explore the response of global extreme precipitation to $CO_2$ forcing in terms of hysteresis and reversibility effect and associated population exposure. In this regard, climate outputs under two idealized $CO_2$ scenarios such as ramp-up (RU; about +1% annually until quadrupling of present level) and ramp-down (RD; around −1% annually set back to present level) from Community Earth System Model version 1.2, and the projected population data from the five shared Socioeconomic Pathways (SSPs) are used. Extreme precipitation events are evaluated using the number of heavy precipitation days (R30 mm), maximum consecutive 5-day precipitation (Rx5day), and the precipitation of very wet days (R95pTOT) indices. Results show that the magnitude of extreme precipitation change and associated population exposure is higher in the $CO_2$ reduction period (RD) than in RU. All the indices show substantial irreversible and hysteresis effects, ~69% of the global land is expected to experience irreversible changes in extreme precipitation. Further, the hotspots of irreversibility (the region with irreversible change and a large hysteresis) will emerge in >20% of the global area. Spatially, strong hysteresis and irreversibility are particularly concentrated over global land monsoon regions. The leading exposure is estimated under SSP3 combined with both RU and RD periods. Under the SSP3-RD combination, the highest population exposure is estimated at ~67.1% (globally averaged), and ~72% (averaged over hotspots) higher than that of the present day. The exposed population is prominent in South Africa and Asia. Notably, the population change effect is the principal factor in global exposure change, while it is the climate change effect over the hotspots of irreversibility. These findings provide new insight into policymaking that only $CO_2$ mitigation effort is not enough to cope with extreme precipitation, rather advanced adaptation planning is a must to have more socio-economic benefits.

## 1. Introduction

Anthropogenic carbon dioxide ($CO_2$) has been the pivotal determinant of an unequivocal global surface temperature increase since the industrial rebellion (IPCC et al., 2013). The rapid upsurge in atmospheric $CO_2$ concentration triggered the change in the Earth's climate system to a more severe, rampant, and irreversible state, causing immense socioeconomic risks (IPCC et al., 2018). To abate such risks, the Paris Agreements set up an ambitious goal to lock global temperature rise well below 2.0 °C (reasonably 1.5 °C) through greenhouse gas (GHG) emission cuts. However, it is expected that even though atmospheric $CO_2$ concentration is reduced (restored to the pre-industrial state), the climate system may not reappear to its initial condition. Particularly, the global climate system is likely to follow a discrete pathway for the $CO_2$ emission and deletion phase. To apprehend such changes in the climate system concerning carbon dioxide removal (CDR) trajectory is fundamental for designing an effective climate change mitigation and adaptation plan (Keller et al., 2018).

The response of the earth's climate system in a CDR trajectories could reflect the hysteresis effect and reversibility change (Skific et al.,

* Corresponding author. Department of Atmospheric Sciences/Irreversible Climate Change Research Center, YonseiUniversity, Seoul, South Korea.
*E-mail address:* sian@yonsei.ac.kr (S.-I. An).

https://doi.org/10.1016/j.wace.2023.100561
Received 14 February 2023; Received in revised form 6 April 2023; Accepted 9 April 2023
Available online 10 April 2023
2212-0947/© 2023 The Authors. Published by Elsevier B.V. This is an open access article under the CC BY-NC-ND license (http://creativecommons.org/licenses/by-nc-nd/4.0/).

2009; Lu and Cai, 2010; Caldeira and Myhrvold, 2013; Keller et al., 2018; Kim et al., 2022). Hysteresis can be demarcated as a reliance on the state of a climate system on its history. For instance, adopting how warm and cold it was in the past, after a certain period, it can be a distinct state of the climate system at the same GHG concentration or temperature. Likewise, reversibility is the ability of the Earth's climate system to be restored to its original state; when it returns to its initial condition known as reversible change, and the opposite case reflects irreversible change (An et al., 2021a,b; Yeh et al., 2021; Kug et al., 2022). Irreversibility of a climate structure can transpire when a climatic variable undergoes a threshold specifically as a 'tipping point' or when the response spans of that variable is comparatively more extensive than that of the forcing timescale (An et al., 2021a,b; Armstrong McKay et al., 2022; Kim et al., 2022). Notably, such irreversibility of a climate system typically consorts the hysteresis effect. However, a series of researches on climate reversibility and hysteresis effect have been carried out based on the Carbon Dioxide Removal Model Inter-comparison Project (CDRMIP) (Keller et al., 2018). Several previous studies explored reversibility and hysteretic effect in the Atlantic Meridional Overturning Circulation (Rahmstorf et al., 2005; Hawkins et al., 2011; An et al., 2021), Antarctica Ice Sheet (Pollard and DeConto, 2005; Garbe et al., 2020), East Asian monsoon (Jo et al., 2022; Song et al., 2022), mean surface temperature (Wu et al., 2010; Cao et al., 2011; MacDougall, 2013; Zickfeld et al., 2016); Intertropical Convergence Zone (Kug et al., 2022), sea level (Boucher et al., 2012), El Niñno-Southern Oscillation (Ohba et al., 2014), and global mean precipitation (Wu et al., 2010; Cao et al., 2011; Chadwick et al., 2013). Importantly, Kim et al. (2022) revealed an extensive irreversible change in global monthly mean surface temperature and precipitation at the regional scale. In view of these previous studies, the research on how reversibility and hysteresis could occur in different climate-change-related extreme events (i.e. extreme precipitation events) is still limited. Recently, Jo et al. (2022) examined the hysteresis behavior in extreme precipitation and reported that the summer count of days when precipitation $\geq$30 mm (R30 mm) indicates an asymmetric response to $CO_2$ forcings over east Asia. Oh et al. (2022) stated that land monsoon precipitation shows contrasting hysteresis behavior in Northern Hemisphere, while extreme precipitation explores slight temporal asymmetries in response to $CO_2$ forcings. However, these past studies highlight the lack of pivotal information availability in the existing scientific literature, especially on how reversibility and hysteresis happen in precipitation-related extreme events at the global and regional scales. Therefore, it has been a great concern to understand the reversibility and hysteresis effect in climate-change-related different extreme (i.e. especially extreme precipitation) for assessing prospective risks and advantages of mitigation scenarios.

Precipitation-related extreme event is recognized as one of the pivotal determining factors of natural disasters globally such as extensive flooding, droughts, landslides, and debris flows, resulting in a colossal and abrupt threat to the social, human, economic, and natural systems (Alexander et al., 2006; IPCC et al., 2013; Zhang and Zhou, 2019; Peng et al., 2020; Paik et al., 2020). Observed evidence suggests a substantial intensification of precipitation-related extremes worldwide since the 1950s (Trenberth et al., 2007; Westra et al., 2013; Pinskwar et al., 2019). Such extremes are also predicted to escalate further in the future under a changing climate. A large number of past studies based on global climate models (GCMs) suggested that the frequency, intensity, and impact area of precipitation-related extremes are expected to upsurge significantly (Fischer et al., 2013; IPCC et al., 2013; Chen and Sun, 2021). It is to be highlighted that precipitation-related extremes exhibit strong regional disparities under global warming scenarios (Trenberth, 2011; Westra et al., 2013; Donat et al., 2016; IPCC et al., 2018; IPCC et al., 2021). A significant increasing trend in extreme precipitation is reported over the Southern Hemisphere such as northern middle and high latitudes and the tropical and sub-tropical, whereas the tropical and subtropical areas of the Northern Hemisphere shows declined trend (Trenberth et al., 2007; Trenberth, 2011). It is expected that such intensified magnitude and spatial variations are likely to affect many people and the economy (gross domestic product; GDP) worldwide, as well as growing disaster risk (Carleton and Hsiang, 2016; Ceola et al., 2014). The latest assessment report (AR6) of the Intergovernmental Panel on Climate Change (IPCC) has underlined that anthropogenic climate change largely influences the changes in extreme precipitation and associated impacts. Therefore, a comprehensive assessment of extreme precipitation in response to CDR has been crucial for measuring future vulnerability and related risks.

Disaster risk is grounded by the interaction of hazard, exposure, and vulnerability, where vulnerability is demarcated as the function of the exposure, sensitivity, and capacity of society to cope with hazard (Field et al., 2012). Besides, exposure is demarcated as the existence of people, economic and social assets, livelihoods, ecosystems, services, and resources in a place and setting that could be affected severely (IPCC et al., 2013). Thus, assessing socioeconomic exposure to climatic extremes has been a growing concern for the scientific community. So far, there are a series of studies conducted focusing on socioeconomic exposure to extreme precipitation (Chen et al., 2020; Liu et al., 2020; Chen and Sun, 2021; Zhang et al., 2018; Zhao et al., 2021; Shi et al., 2021; Mondal et al., 2022; Ayugi et al., 2022). Most of the previous studies are carried out based on the different phases of Coupled Model Inter-comparison Project (CMIP) (i.e. CMIP3, CMIP5, and CMIP6), and reported increased population and GDP exposure to extreme precipitation with continued warming or GHG emission. However, researches on whether and how the socioeconomic risk of extreme precipitation would respond to decreased $CO_2$ are still unknown. In particular, how population exposure to extreme precipitation will evolve in the future if anthropogenic $CO_2$ emission is removed or stabilized to its initial state? Here, we reasonably assume that the population will not follow the decreasing path of $CO_2$ concentration. Therefore, a robust assessment of socioeconomic exposure to future extreme precipitation concerning CDR scenarios is crucial for adaptation and mitigation approaches.

This study endeavors some new aspects compared with the previous works. Notably, this study explores hysteresis and reversibility effect of extreme precipitation focusing on different climatic zones. We know that weather and climate do not respect any political boundaries. Thus, the analysis of the precipitation extreme emphasizing different climatic zone will assist in an intense understanding of the global impact of climatic systems over the region. Further, this study considers multiple broadly acceptable extreme precipitation-related indices to reveal more reliable and reasonable findings. Importantly, this study detects the global hotspots of the irreversibility of extreme precipitation change and estimates changes in prospective population exposures. In light of these issues, this study aims to assess the reversibility and hysteresis effect in precipitation-related extreme events concerning anthropogenic $CO_2$ forcing and associated population exposure. Notably, this study emphasizes detecting hotspots of irreversible changes in global precipitation-related extreme events. Further, this study focuses on quantifying the population exposed to extreme precipitation considering the three causal factors such as population change effect, climate change effect, and their interaction effect (population and climate change happens simultaneously). Here, extreme precipitation events are explored by adopting three broadly used indices such as the number of heavy precipitation days (R30 mm), maximum consecutive 5-day precipitation (Rx5day), and the precipitation of very wet days (R95pTOT) as demarcated by the Expert Team on Climate Change Detection and Indices (ETCCDI). Further, most of the previous studies reported regional variations of hysteresis and reversibility. So, the prospective changes of reversibility and hysteresis effect in the precipitation-related extreme are carried out over five major climatic zones such as tropical, temperate, arid and semi-arid, cold, and polar zone (based on Köppen–Geiger classification) (see Fig. S1). For our analysis, we designed an idealized $CO_2$ ramp-up and ramp-down experiment where atmospheric $CO_2$ level upturns from 367 ppm (initial state; present-day level) to 1 468 ppm (increased four times with the rate of 1% per each

year), afterward declined back to its initial level (367 ppm) at the same rate. This CDR experiment is conducted with the Community Earth System Model (CESM1.2) with a total of 28 ensemble members.

## 2. Materials and methods

### 2.1. Climate model experimental structure and dataset

In this study, climate model outputs of the CDR experiment are analyzed by adopting the fully coupled Community Earth System Model version 1.2 (CESM1.2; Hurrell et al., 2013). The CESM1.2 comprises multiple modeling dimensions such as the atmospheric model (the Community Atmospheric Model version 5; CAM5) with a ~1° × 1° horizontal resolution (Neale et al., 2010), oceanic model (the Parallel Ocean Program version 2; POP2) which has a horizontal resolution of 1° × 0.3° (Smith et al., 2010), the Community Ice Code version 4 (CICE4) is the ice-sea model secure ~1° × 1° resolution (Hunke and Lipscomb, 2010), and the land model named as the Community Land Model version 4 (CLM4) with a ~1° × 1° horizontal resolution (Lawrence et al., 2011). Notably, this CESM experiment is compared to CDRMIP (Keller et al., 2018) which is developed as part of the latest sixth phase of Coupled Model Inter-comparison Project (CMIP6) to reveal the irreversible changes and hysteresis effect in response to $CO_2$ reduction. The only basic difference between these two experiments is the primary $CO_2$ level consideration.

A series of simulation experiments are defined considering different $CO_2$ levels such as present-day (PD), ramp-up (RU), ramp-down (RD), and restoration periods (An et al., 2022; Fig. S2). The PD simulation experiment is set up from a fixed 367 ppm $CO_2$ level (i.e. present state) for more than 900 years. In the RU simulation, the atmospheric $CO_2$ level is considered to increase from 367 ppm to 1 478 ppm (four times higher than the PD) at a 1% rate per year for the next 140 years (ranges 2001–2 140), whereas the atmospheric $CO_2$ level is symmetrically reduced back from 1 478 ppm to its initial condition 367 ppm in the RD phase at the same ~1% rate per year for next 140 years (2141–2 280). Followed by the RD period, atmospheric $CO_2$ concentration is considered to be fixed as its primary state (367 ppm) for the next 220 years which is called the restoration phase. Besides, a total of 28 ensemble members for each experiment (except PD) are produced, and here we displayed the ensemble-mean results. For more detailed information can refer to An et al. (2021). However, in this study, we used the daily precipitation (mm $day^{-1}$) variable from this experiment for PD, RU, and RD phases. Particularly, the PD period in this study is considered from 1975 to 2000 when we are estimating extreme precipitation frequency and associated population exposure.

Further, to quantify the socioeconomic impact of extreme events in terms of population exposure to extreme precipitation, this study used gridded future population data encapsulated under the five socioeconomic scenarios called Shared Socioeconomic Pathways (SSPs). The five socioeconomic scenarios are known as sustainability (SSP1), middle-of-the-road (SSP2), regional rivalry (SSP3), inequality (SSP4), and fossil-fueled development (SSP5). The SSP1, SSP2, and SSP3 scenarios signify low, intermediate, and high societal vulnerability, whereas SSP4 and SSP5 denote high challenges for adaptation, and mitigation, respectively (O'Neill et al., 2014). In this study, the gridded population data for the base year (i.e. 2000) and five SSPs (from 2010 to 2 100) are downloaded from Socioeconomic Data and Applications Center (SEDAC) website (https://sedac.ciesin.columbia.edu/). More details about the SSPs-based projected spatial population distribution can be found in Gao (2020). Notably, we considered a common resolution (i.e. 1° × 1°) for both the climate and population data. To resample population data into the common resolution of 1° × 1°, we used the "nearest grid" interpolation method which is adopted from the Matlab function 'interp2'.

### 2.2. Methods

#### 2.2.1. Extreme precipitation metrics

Defining extreme precipitation events is somewhat challenging due to the more diverse and complex features of precipitation change over the world (IPCC et al., 2013). However, a set of extreme precipitation metrics have been well-defined by the ETCCDI. Typically, such indices can be classified into three major types such as intensity, frequency, and duration. In this study, widely accepted and broadly used three extreme precipitation indices are selected such as the number of heavy precipitation days (R30 mm), maximum consecutive 5-day precipitation (Rx5day), and the precipitation of very wet days (R95pTOT). Where R30 mm indicates the frequency of extreme precipitation, and Rx5day and R95pTOT represent intensity. Notably, the R95pTOT in this study is considered as the annual sum of precipitation in days where daily precipitation exceeds the 95th percentile of daily precipitation in the present day period (1975–2000).The specific definition of these metrics is demarcated in Table 1.

#### 2.2.2. Measuring the hysteresis area, and reversibility

The climate trajectory of a given climate variable (i.e. precipitation) in response to $CO_2$ forcing can evolve in various ways, and the most possible dimensions are hysteresis area, and reversibility. To better depict these phases, a conceptual framework is developed by Kim et al. (2022). These concepts are adopted in this study to quantify hysteresis area, reversibility, and openness. For CDR scenarios, the $CO_2$ concentration in the atmosphere (F) is expected to inflate from the PD level ($F_{present}$) to the utmost in the future ($F_{peak}$). In response to $CO_2$, the changes in climate trajectory are expected to be different during the period of $CO_2$ upturn ($x_{up}$) and shrinkage ($x_{down}$), only if the system demonstrates hysteresis. Notably, the positive value of the absolute difference between ($x_{up}$) and ($x_{down}$) signifies the hysteresis area. Whereas, reversibility is regarded as the ability of the trajectory whether it is set back to its primary condition; if it returns to its initial state indicated as a closed-loop (reversible change), if not, it signposts an open-loop (irreversible change). More detailed explanations of hysteresis area, reversibility, and different loop types featured by the hysteresis area and openness can be referred to Kim et al. (2022).

In our investigation, we estimated the grid-wise hysteresis area (A) and loop openness of precipitation-related extreme events (R30 mm, Rx5day, and R95pTOT). If the system does not reflect any hysteresis, it will signpost no hysteresis area (A = 0) as well as indicates closed-loop. To ensure the diminished internal variability as well as represent a more concrete response to $CO_2$ forcing, the ensemble mean of 28 experiments is used in this study both for the ramp-up and ramp-down. Here, the hysteresis area (A) and loop openness for each grid point in this study using the following equation (Kim et al., 2022):

$$A = \int_{F_{prsent}}^{F_{peak}} \left| x_{down}(F) - x_{up}(F) \right| dF \quad (1)$$

For loop openness/closeness, we expected that the trajectories do not cross each other during the period of $CO_2$ upturn ($x_{up}$) and shrinkage ($x_{down}$), they can only meet at the lowermost $CO_2$ level (i.e. present $CO_2$

**Table-1**
The demarcations of the nominated indices.

| Extreme precipitation Index | Definition | units |
|---|---|---|
| R30 mm | The cumulative number of precipitation days with ≥30 mm of precipitation | days |
| Rx5day | Maximum consecutive precipitation amount in 5-day precipitation | mm |
| R95pTOT | The annual total amount of precipitation during days in which daily precipitation exceeds the 95th percentile of the wet-day precipitation | mm |

level; $F_{present}$) if the loop is closed. But the trajectory also signifies that several grid points can intersect at the intermediate $CO_2$ level (i.e. 1 300 ppm; $F_{mid}$), which is also reasonable to be considered a closed-loop. However, more straightforwardly, if the difference between ramp-up and ramp-down becomes larger than zero (>0) is considered an open-loop (irreversibility), whereas ≤0 is taken as a closed-loop (reversibility). The loop openness of the trajectory is estimated using the following equations (Kim et al., 2022):

$$Loop = \begin{cases} Open\ for\ min\left(x^*_{up} - x^*_{down}\right) \times max\left(x^*_{up} - x^*_{down}\right) > 0 \\ Closed\ for\ min\left(x^*_{up} - x^*_{down}\right) \times max\left(x^*_{up} - x^*_{down}\right) \le 0 \end{cases} \quad (2)$$

Here, $x_{up}$* and $x_{down}$* are the ramp-up and ramp-down trajectories for the period of $CO_2$ level from $F_{present}$ to $F_{mid,}$ respectively. If the system intersects at this range is a closed-loop, if they do not is called an open-loop.

### 2.2.3. Defining the hotspots of irreversible change

The hotspots of irreversible changes over the global land are identified considering all the selected extreme precipitation indices. The identified hotspots for irreversible changes are defined as the land area where all the selected precipitation-related extremes (index; R30 mm, Rx5day, and R95pTOT) show an open-loop response (irreversible change) and a large hysteresis area (>90th percentile).

### 2.2.4. Exposure assessment

As stated by the United Nations International Strategy for Disaster Reduction (UNISDR, 2017), population exposure to extreme precipitation can be defined as the number of populations in geographical locations and setting that can be adversely affected by precipitation-related extreme events. According to Jones et al. (2015), numerically, population exposure to extreme precipitation can be measured by multiplying the frequency of an extreme precipitation event by the number of people in an extremely precipitation-prone area. Notably, the selected frequency index (R30 mm); annual maximum days with precipitation ≥30 mm is considered to estimate population exposure in this paper. The extreme event-based hazard is typically grounded by the geographical structure, physical features of the event, and the magnitude of change, infrastructure status, and awareness of the community. A large amount of precipitation can lead to more adverse floods and landslides, such fixed value-based index (i.e. R30 mm) reflects more dangerous circumstances in the local distinct environment (Zhan et al., 2019; Shen et al., 2022). To better quantify the population exposure, we explored exposure under all the possible combinations. The projected population for all the selected SSP scenarios is combined with extreme precipitation frequency under both the RU and RD periods. For instance, we combined extreme precipitation frequency under the RU period with all the SSPs; SSP1-RU, SSP2-RU, SSP3-RU, SSP4-RU, and SSP5-RU. Same for the RD period. As the timeframe for available population projections under SSPs and extreme precipitation under are not consistent (as SSPs population data after 2 100 is not available), at first, we averaged population over 90 years period (i.e. 2010-2100) as well as the frequency for both the RU and RD periods averaged over 140 years (RU; 2001–2140, and RD; 2140–2 280), then spatially combined to estimate exposure. Besides, the identical population level (i.e. 2010-2100) is further considered for both RU and RD periods. We assumed that the population in the long future (after 2 100) might follow any one of the five SSPs, hence we considered all the possible combinations that figure out the diverse outlook of expected exposure. Similar broad combinations were also reflected in a study by Zhang et al. (2018). However, statistically, population exposure to extreme precipitation at each grid can be expressed as:

$$E_{i,} = P_i \times F_{i,} \quad (3)$$

Where, $E_{i,}$ denotes the population exposed at grid *i*th to extreme precipitation hazard (i.e. R30 mm). $P_i$ signifies the number of population at grid *i*th, and $F_{i,}$ is the frequency of extreme precipitation at grid *i*th.

### 2.2.5. Influential factor in exposure change

Three key causal factors mostly influence the changes in exposure. Jones et al. (2015) stated that the population exposure change (ΔE) is expected to be decomposed into three factors such as population change effect ($CR_{pop}$), climate change effect ($CR_{cli}$), and population-climate interaction effect ($CR_{int}$) (population and climate change happens simultaneously). The changes in the total population exposed to the extreme event could be decomposed by the following equation:

$$\triangle E = C_i \times \triangle P + P_i \times \triangle C + \triangle P \times \triangle C \quad (4)$$

However, the relative contribution of each factor can be calculated based on the following equations:

$$CR_{pop} = \frac{C_i \times \triangle \mathrm{P}}{\triangle E} \times 100\% \quad (5)$$

$$CR_{cli} = \frac{P_i \times \triangle \mathrm{C}}{\triangle E} \times 100\% \quad (6)$$

$$CR_{int} = \frac{\triangle \mathrm{P} \times \triangle \mathrm{C}}{\triangle E} \times 100\% \quad (7)$$

Where, ΔE is the total exposure change, $C_i$ signifies the extreme precipitation frequency in the historical period, and $P_i$ is the historical population status. ΔP and ΔC denote the future population change and extreme precipitation frequency change concerning the historical period.

## 3. Results

### 3.1. Hysteresis and reversibility of extreme precipitation

In this section, we explored the changes in hysteresis and reversibility of three selected extreme precipitation indices (i.e. R30 mm, Rx5day, and R95pTOT) over the globe and five climate regions in response to $CO_2$ forcing. Spatial information of five climate regions is presented in the supplementary materials (Fig. S1). The evolution of these three indices for RU and RD periods are firstly investigated (shown in supplementary materials; Fig. S4). Where, the difference value (average) between ramp-up and ramp-down indicates the existence of hysteresis (value > 0 indicates hysteresis, and ≤0 specifies no hysteresis). The significant existence of hysteresis (difference between RU and RD periods) is tested using the one sample *t*-test. Followed by, the spatial distribution of the hysteresis area with closed-loop (reversible change) area as well as its regional quantity are also presented here (Fig. 1). In Fig. 1, the change in hysteresis area for each grid point of the extreme precipitation indices is calculated using equation (1), and the irreversibility of extreme precipitation is designed based on equation (2).

The prospective changes in areal averaged annual R30 mm, Rx5day, and R95pTOT for the RU and RD periods over the globe and five climate regions are presented in Fig. S4. Overall, the annual feature of all the studied indices (R30 mm, Rx5day, and R95pTOT) are subjective to intensify with $CO_2$ upturn for both the ramp-up and ramp-down scenarios in the global and regional aspects, where the magnitude of change is higher in the ramp-down scenario than that of RU (Figs. S4a,b, and c). Individually, R30 mm demonstrates significant hysteresis in the globe and its climatic zones, except for the polar region (Fig. S4a). Overall it shows an open-loop reaction over the global land, where the closed-loop response is likely to transpire in the polar climate zone. Likewise, Rx5day overall explores a significant hysteresis globally but there is a regional disparity (Fig. S4b). Though the tropical, temperate, and polar climate exhibit significant hysteresis, the hysteresis is not significant over arid and cold regions. Similarly, R95pTOT is also envisioned to

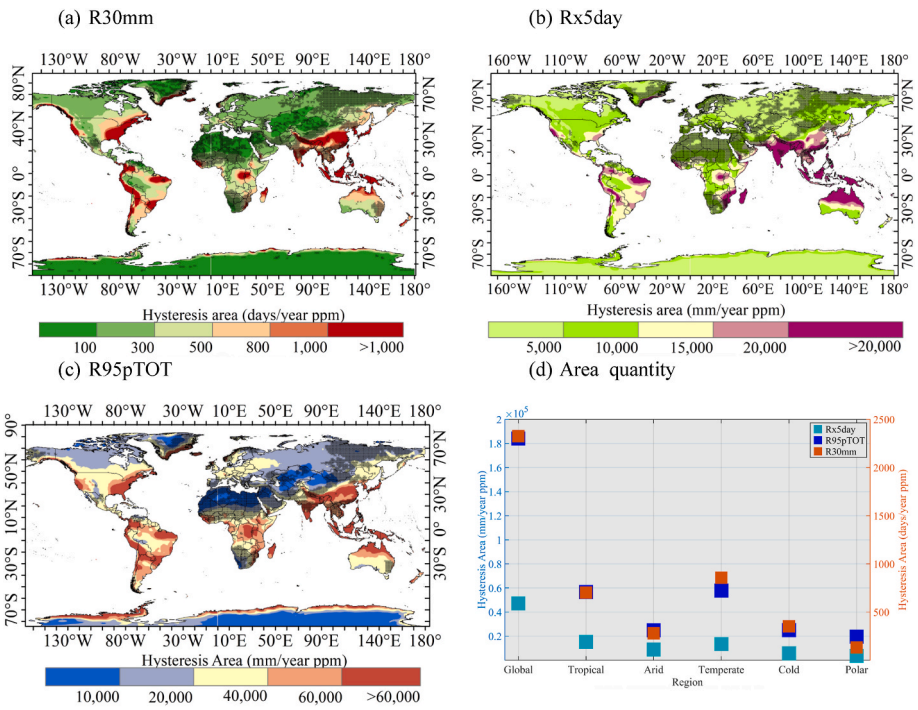



**Fig. 1.** Spatial structure of hysteresis area of (a) R30 mm, (b) Rx5day, and, (c) R95pTOT in response to $CO_2$ forcing over the globe, and (d) Region-wise hysteresis area quantity; where left y-axis denotes changes of Rx5day and R95pTOT, and the right y-axis indicates R30 mm change. Shaded indicates area with closed-loop.

yield significant hysteresis for both global and regional levels with an open-loop tendency in response to $CO_2$ change (Fig. S4c). So, it is evident that extreme precipitation events are inclined to exhibit extensive hysteresis and irreversible changes globally in the future, where regional variation is obvious.

The spatial structure of the hysteresis area of the selected indices is determined in Fig. 1. The spatial distribution of the hysteresis area of all the indices (R30 mm, Rx5day, and R95pTOT) over the globe mostly shows a consistent pattern, especially for the leading change area. Individually, the extreme event exhibits substantial regional variation in changes in hysteresis area as well as reversibility (open-loop) (Fig. 1a). The largest hysteresis area (≥1 000 days/year ppm) of R30 mm mostly emerges over South Asia, Southeast Asia, and part of America. Similarly, the prominent area (≥20,000 mm/year ppm) of Rx5day is mostly dominant over South Asia, Southeast, and Northeast Asia, and part of Australia (Fig. 1b). In the same way, R95pTOT exhibits a dominant hysteresis area (≥60,000 mm/year ppm) over South Asia, Southeast, and Northeast Asia, part of Australia, South Africa, and South America (Fig. 1c). Furthermore, for the hysteresis area quantity of all the indices in different climate regions (Fig. 1d), the temperate climate region is expected to have the largest hysteresis followed by the tropical region, whereas the lowest hysteresis found in the polar climate region. The R95pTOT shows the highest magnitude of change, followed by Rx5day, and the lowest one is R30 mm. Further, to better reflect the spatial feature of irreversible change, the area with open-loop globally is considered (shaded area; Fig. 1a, b, and c). Approximately 57%, 75%, and 76% of the global area are expected to experience irreversible change (open-loop) for R30 mm, Rx5day, and R95pTOT respectively. For different climatic zones, more than 90% area of the polar climate region is expected to undergo open-loop response for R30 mm and R95pTOT, whereas it is 74% area of the temperate zone for Rx5day. Moreover, the hysteresis area is dominant in the region with irreversible change (Fig. S5). So, it can be highlighted the majority of the global land is prone to experience irreversible changes in extreme precipitation (~69% of the global land; average area of all the three indices).

### 3.2. Detecting the hotspots of irreversible change

In this section, we identify future hotspots for irreversible change in extreme precipitation events over the global land in response to $CO_2$ forcing (Fig. 2). A comprehensive approach is applied to detect the area where the widespread hysteresis and irreversibility effect in extreme precipitation is obvious in extreme precipitation. The hotspots are identified based on the estimated hysteresis area and irreversible response (open-loop) of the selected three extreme precipitation indices. The hotspots for irreversible change in extreme precipitation are determined as the land area where all the indices exhibit an open-loop feedback securing an area with >90 percentile.

Fig. 2 demonstrates the major prospective hotspots for irreversible change in extreme precipitation over global land in response to atmospheric $CO_2$. Under the adopted idealized $CO_2$ emission pathway, hotspots area evolves over more than 20% of the global land. Areas in South Asia, Southeast and Northeast Asia, Australia, South Africa, South, and North America, and coastal regions of Antarctica are detected as hotspot regions. Specifically, the hotspots transpire largely in most of the developing countries such as India, China, Bangladesh, Myanmar, and Indonesia situated in Asia. Developing countries in America and South Africa such as Chile, Peru, Ecuador, Brazil, Uruguay, Mozambique, Madagascar, and Zambia are further identified as hotspots. In contrast, hotspots also emerge in some developed countries around the world such as the United States, Canada, Australia, South Korea, and New Zealand. Moreover, the areas covered with ice sheets, and the coastal land of Antarctica, Greenland, and Alaska are similarly identified as the prospective hotspots.

### 3.3. Population exposure to extreme precipitation

It is pivotal to scrutinize the spatiotemporal distribution of hazards and population before estimating associated exposure. The spatial structure of the number of extreme precipitation days (based on the R30 mm) under RU and RD periods as well as present-day are illustrated in Fig. 3. Whereas the overall change in the population under five SSPs is shown in the supplementary document (Fig. S6)

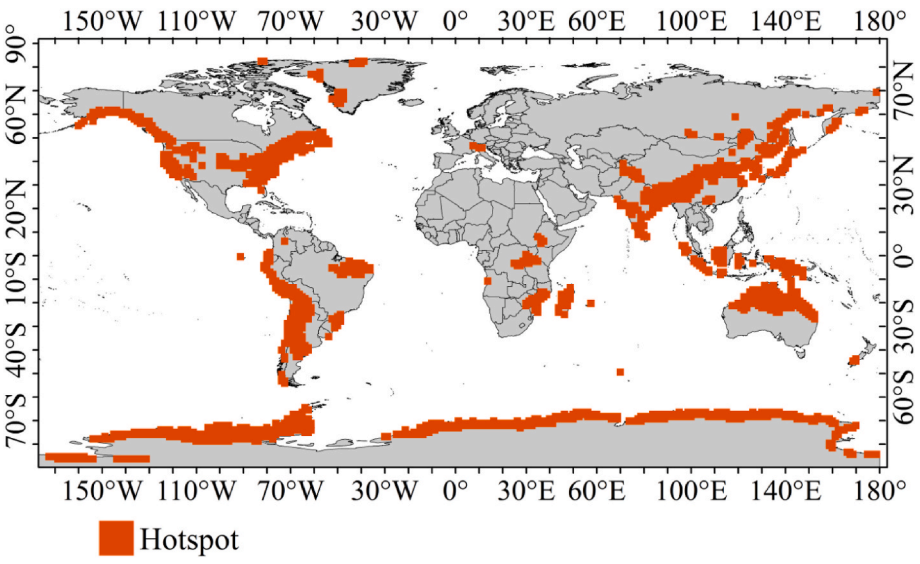



**Fig. 2.** Global hotspots of irreversible changes in extreme precipitation events.

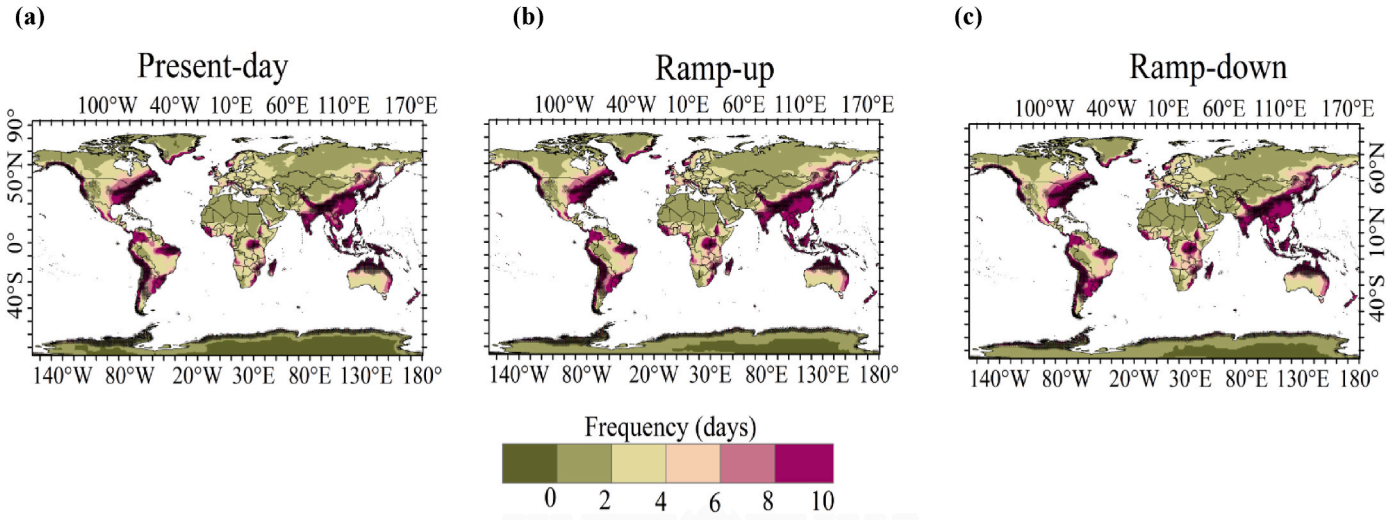



**Fig. 3.** Prospective changes in the frequency of global extreme precipitation for (a) present-day, (b) ramp-up, and (c) ramp-down periods. The shaded area indicates hotspots regions for irreversibility in extreme precipitation.

*3.3.1. Changes in frequency of extreme precipitation*

The projected changes in the number of extreme precipitation days are inclined to increase from present-day (1975–2000) to future scenarios (RU, and RD), where the highest frequency is recorded under the ramp-down scenario (Fig. 3). The average frequency in the present-day is 3.8 days, while it is 4.0 (~5% higher than PD) and 4.2 days (~10% higher than PD) under RU and RD scenarios, respectively. In the spatial aspects, although the prospective changes in extreme precipitation frequency exhibit a consistent escalation globally, they demonstrate strong regional features in the future standpoints. Precipitation-related extreme events are intended to transpire most recurrently over a wet tropical climate region adjacent to the equator. Under the $CO_2$ idealized RU and RD scenarios, the projected increase in the frequency of extreme precipitation (≥10 days) is mainly distributed in monsoon regions such as southern-, southeastern- and northeastern Asia, part of southern-, and northern America, southern Africa, and northern Australia. Though the distribution of extreme precipitation frequency for the PD and future periods shows a consistent pattern, the quantity of area with the highest number of days (≥10 days) with the extreme event is slightly higher towards the RD period. The area with the highest frequency (≥10 days) is estimated at 9.1%, 10.7%, and 11.6% of the global land for PD, RU, and RD periods. Further, it can be noted, extreme precipitation is even more predominant in the hotspots of irreversible change (shaded area; Fig. 3), where the average frequency is 12.2, 14.3, and 16.2 days for PD, RU, and RD periods, respectively. Around 40.1%, 46.9%, and 55.7% of the total hotspot area are expected to experience more frequent extreme precipitation at a rate of ≥10 days per year for PD, RU, and RD periods, respectively. However, it can be boldly written that global land is expected to incur the most frequent extreme precipitation event during the RD period, which is ~10% higher than that of the PD (global average), and it reaches ~32% in the hotspots area. This outlook of the changes signifies that only $CO_2$ mitigation is not enough to decrease such extreme event occurrence rates. Spatially, the monsoon regions are prone to experience such extreme events more frequently. Further, the hotspots of irreversibility change are the most vulnerable area to suffer from such extreme events.

*3.3.2. Changes in the population exposed to extreme precipitation*

To detect the anticipated impacts of precipitation-related extremes over the globe, the population exposure is determined by combining the

spatial distribution of hazards and the corresponding population. In this regard, we considered changes in population over 90 years and climatic change for 140 years. However, population exposure caused by extreme precipitation is estimated under two future periods such as RU, and RD combined with five SSP scenarios as well as for the PD in Fig. 4. For the exposed population aggregated over global lands (Fig. 4a), the global annual population exposed to extreme precipitation in the present-day period is ~38 × $10^5$ person-days. For future standpoints, exposure is estimated to be larger than that of the PD period. Unlikely to future changes in extreme precipitation frequency, the number of people affected by extreme precipitation is projected to increase under both future scenarios. In terms of the scenario comparison, the exposed population is slightly higher in the RD period than the RU for all combinations (Fig. 4a). The number of people exposed to extreme precipitation is projected to be the greatest under the scenario combination of SSP3 with both ramp-up (SSP3-RU combination) and ramp-down (SSP3-RD combination), where the lowest in the combination with SSP1. With regard to the present-day period, the expected exposure is estimated by about 28.5%, 42.3%, 65.2%, 39.5%, and 30.4% higher for all the possible scenario combinations such as SSP1-RU, SSP2-RU, SSP3-RU, SSP4-RU, and SSP5-RU, accordingly. Whereas for the RD period, it reaches around 30.6%, 45.0%, 67.1%, 41.6%, and 32.8% larger than that of PD under SSP1-RD, SSP2-RD, SSP3-RD, SSP4-RD, and SSP5-RD scenario combinations, respectively. Further, the exposed population aggregated over only the hotspots of irreversible change follows a similar increase tendency to global average exposure for all the scenario combinations (Fig. 4b). Notably, the anticipated upsurge in exposure under RD scenario combinations is more predominant than that of RU period. In the PD period, the number of the person exposed to extreme precipitation over the hotspots is ~32 × $10^5$ person-days. In the future aspects, the most rapid increase in exposure over the hotspots is estimated by ~72% higher under the SSP3-RD compared to the PD state, whereas it is ~61% under the SSP3-RU combination. However, the exposure is estimated to be higher under future periods than that of the PD period. The most dominant increase in exposure is expected to transpire under SSP3-RU and SSP3-RD, where the exposure is higher under RD than RU combinations. Statistically, the exposure aggregated over the global total land area (hotspots area) is expected to be 65.2% (~61%), and 67.1% (~72%) higher for RU and RD than the PD, respectively. Both the population and extreme precipitation frequency change are prominent in the hotspots area, hence exposure over hotspots is more dominant in hotspots than that of global average, especially for RD (as extreme precipitation frequency higher for RD).

The spatial distribution of the changes in the population exposed to precipitation-related extremes for the two future periods combined with the five SSPs relative to the current state over global lands is displayed in Fig. 5. In the present-day period (Fig.5Aa and 5Ba), the spatial pattern of exposure shows a similar spreading for both RU and RD periods located

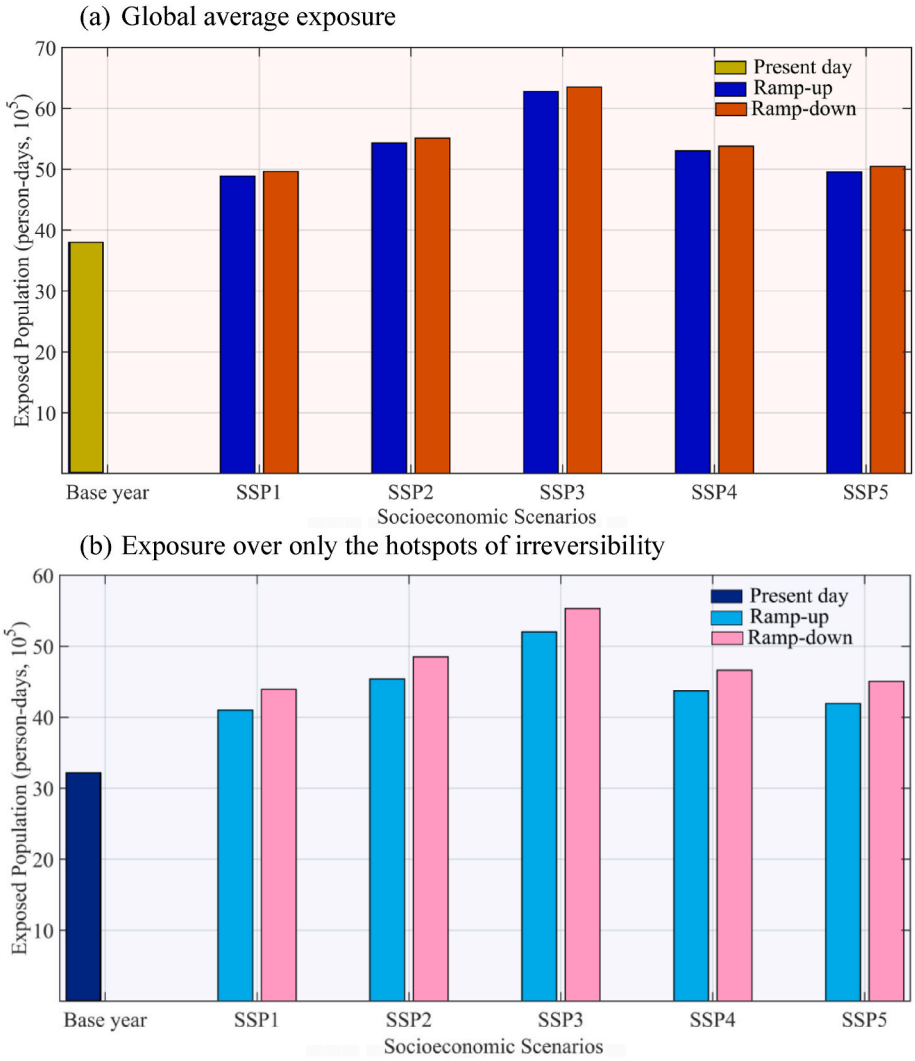



**Fig. 4.** Changes in the population exposed to extreme precipitation for the present-day, ramp-up, and ramp-down periods over the (a) global land area, and (b) hotspots of irreversibility area.

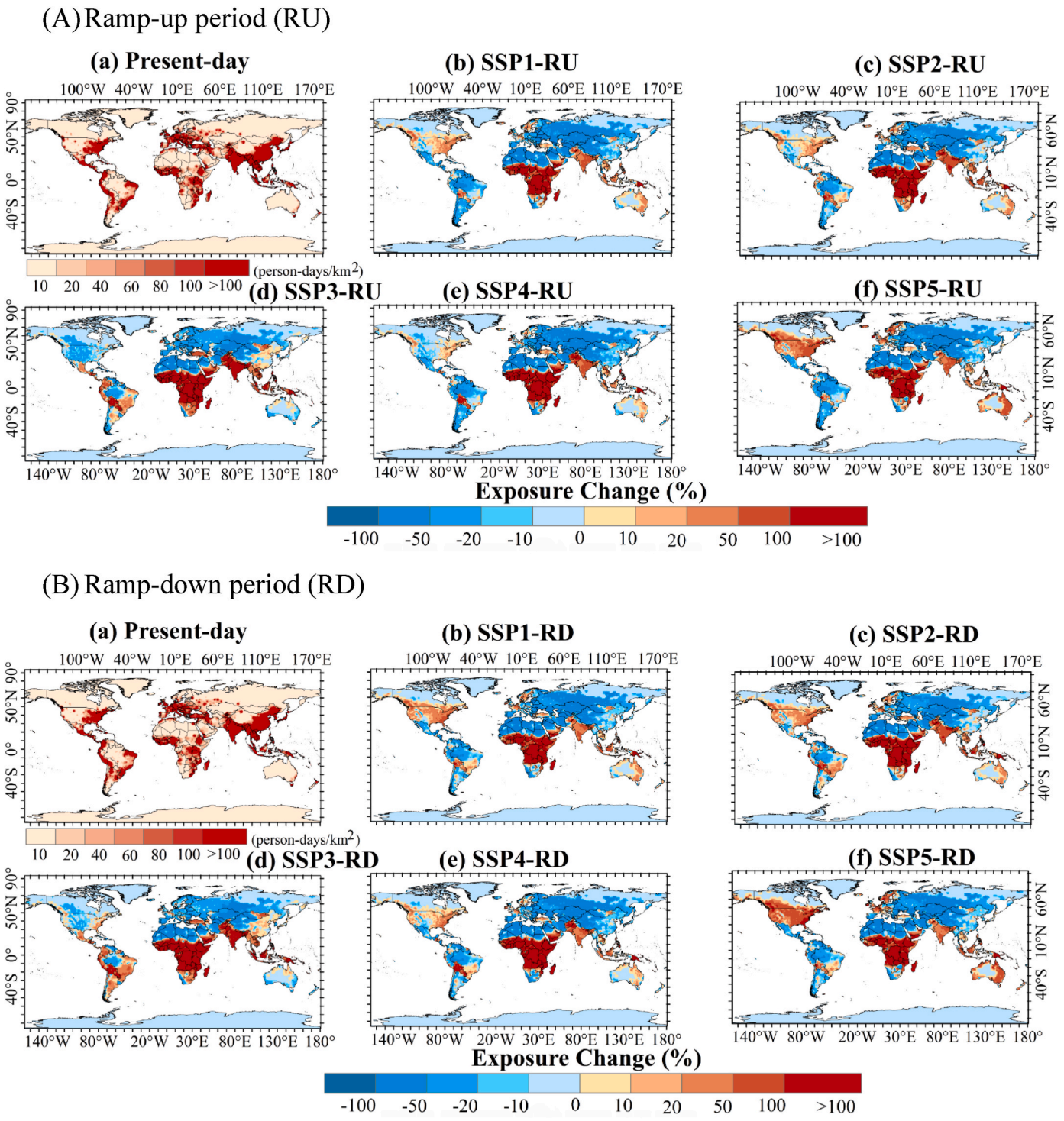



**Fig. 5.** Geographical structure of the population exposed to extreme precipitation under five SSPs scenarios combined with (A) ramp-up, and (B) ramp-down periods with regard to the present-day period.

in densely populated regions. The area with the largest exposure (≥100 person-days/km$^2$) in the PD period is most pronounced in southern-, and eastern-Asia, central- and southern-Africa, central-Europe, northwestern-, and southern-America, and southeastern North-America. For future standpoints, the spatial changes are attributed to the PD period (Fig.5Ab-f, and Bb-f). The geographical distribution of the future population exposure is largely homogeneous under all the selected SSP scenarios combined with RU and RD periods. In relative terms, the exposure is inclined to soar in central-, and southern-Africa mostly as well as southern-, and eastern-Asia for all the scenario combinations. In central-, and southern-Africa the population exposed to extreme precipitation is expected to increase by >100% higher than that of PD for all the scenario combinations. The area with a 100% increase is exhibited in southern-, and eastern-Asia, while it reaches >100% for only SSP3 scenario combinations (SSP3-RU, and SSP3-RD). Such a dominant feature can be caused by the highest population growth under this pathway which poses high social vulnerability. Moreover, future exposure is also prospective to transpire over northwestern-, and southern-

America, southeastern North-America, and Australia. However, it can be loudly speaking that the people located in central-, and southern-Africa, as well as southern-, and eastern-Asia are highly vulnerable to being affected by extreme precipitation in the future with respect to the PD.

The relative contribution of different causal factors that influence changes in future exposure aggregated over the global total land area and hotspots of irreversibility is determined in terms of climate change effect, population change effect, and climate-population interaction effect shown in Fig. 6. The effect of underlying factors in population exposure change exhibits strong regional disparities. For the exposure aggregated over the global total land area (Fig. 6a and b), the population change effect is the principal contributor in exposure change for both the two future periods (RU and RD) combined with the five SSPs. The role of the population change effect is intended to decline slightly and the effect of climate change becomes stronger gradually over time under all the future scenario combinations. The relative importance of the population change effect varies by about 80%–88% among the scenario combinations during the RU period, whereas it is around 67%–80% in the RD period. In contrast, the contribution of the climate change effect is expected to increase from about 7% to 16% in the RU period to 12%–26% during the RD period among the scenario combinations. Notably, the leading contribution of the population change effect is estimated under the SSP3 scenario combined with both RU and RD periods, which is ~88% in the RU, and ~80% for the RD periods. Whereas, the climate change effect is dominant under SSP1 scenario combinations, which is ~16% and ~26% during RU and RD periods (i.e. SSP1-RU and SSP1-RD), respectively. Such findings under SSP1-RU and SSP1-RD signify that the earth's climate will change more rapidly under RU and RD periods than the population change under the lowest growth pathway (SSP1). So, the population change effect is the most predominant contributor to exposure change over the global total land area, followed by the climate change effect. In contrast, for the effect of the causal factors in the exposure aggregated over hotspots of irreversibility (Fig. 6c and d), the climate change effect is the pivotal contributor to exposure change under all the scenario combinations, except for SSP3-based combinations. In the RU period, the relative contribution of climate change effect varies around 30%–57% while it increases towards the RD period by about 42%–69%. It indicates that the effect of climate change is intended to be dominant with time. However, it can be boldly written that the population change effect is the principal contributor to global averaged population exposure change, and it is the climate change effect over the hotspots of irreversibility, while the interaction effect of climate-population has never played the prime role.

## 4. Conclusions and discussions

This study scrutinizes the hysteresis and reversibility of extreme precipitation changes and their resultant impact globally in response to atmospheric $CO_2$ forcing. The hotspots of irreversibility in extreme precipitation and associated socioeconomic impact in terms of population exposure are further investigated. In this concern, CESM1.2 CDR simulations under two idealized $CO_2$ forcing scenarios RU and RD are used. Notably, the ETCCDI-defined three indices (i.e. R30 mm, Rx5day, and R95pTOT) are applied to estimate hysteresis and reversibility in extreme precipitation variations over the global land and its five major climate regions.

Every bit of $CO_2$ concentration matters, the variation in $CO_2$ forcing typically lead to widespread hysteresis and reversibility effect in different global climatic parameters. The findings of this study highlight that the annual changes in three selected extreme precipitation indices (i.e. R30 mm, Rx5day, and R95pTOT) over the global and regional aspects signify consistent wetting tendency with $CO_2$ increase for both RU and RD periods, where the magnitude is higher under RD. The dominant increase under the RD period influences the hysteresis and irreversible effect in extreme precipitation. Among these selected indices, R95pTOT exhibits the highest magnitude of change in hysteresis area quantity, where R30 mm is the lowest one. Further, the global area with irreversible change (open-loop) is also expected to be highest for R95pTOT (76%), while it is 57% for R30 mm. Such findings indicate that the hysteresis and irreversibility effect is longer in the intensity of global extreme precipitation than that of frequency. Further, for different climatic zones, R95pTOT shows significant hysteresis over all the regions, whereas significant hysteresis for Rx5day is found over tropical, temperate, and polar regions (except arid and cold regions), and R30 mm exhibit significant hysteresis over all the regions (except polar region). Such regional disparities of extreme precipitation indices may be influenced by the local climatological and topographical characteristics. However, it is obvious that substantial upturn in the global precipitation-related extreme events in terms of both frequency and intensity is dominant in the $CO_2$ reduction period (RD) period than that of the increase period (RU). Such asymmetric responses also exist in the regional scales (over five major climate regions). This outcome signifies the continued increase of extreme precipitation events (i.e. more frequent and intense) for the next several decades even if atmospheric

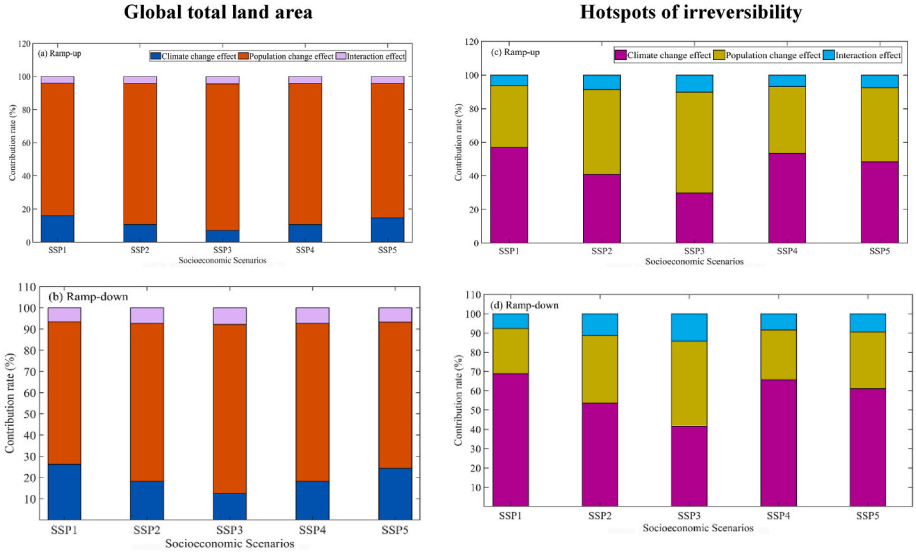



**Fig. 6.** Different causal factors contribute to the changes in population exposure to extreme precipitation for the two future periods (RU and RD) aggregated over the global total land area (a–b), as well as hotspots of irreversibility (c–d).

$CO_2$ concentration is reduced. As a result, global socioeconomic risk and immense damages caused by extreme precipitation events are prospective to an upsurge in the long future under net-negative $CO_2$ emission. In general, it is assumed that the rapid reduction in $CO_2$ will lead to slowing the climate change process resulting in smaller risks. But our findings prove that this assumption is inappropriate in aspects of $CO_2$ emission. Similar findings were also reported by Jo et al. (2022) that the R30 mm is expected to increase over East Asia even if after reducing atmospheric $CO_2$ concentration. However, this asymmetric response can be clarified by the rapidity of mitigation of $CO_2$ and global average temperature (Wu et al., 2010; Cao et al., 2011). Further, Jo et al. (2022) indicated that a persisted El Niño-like warming in the RD period influences the asymmetric response of extreme precipitation through northwestward propagating wave response and a tri-pole structure (positive-negative-positive) in extreme precipitation frequency. It is also explored that the response of mean precipitation change and extreme precipitation concerning $CO_2$ forcing differ to some extent (Fig. S3; Oh et al., 2022). Moreover, as the world receives most rainfall in the summer season and extreme precipitation events also occur in this season, it is expected that the hysteresis effect of extreme precipitation would be more dominant in the summer than that of winter. Some previous study already explored the seasonality of hysteresis. Kim et al. (2022) stated that the seasonal precipitation patterns largely differ from the annual mean where the largest hysteresis and the irreversible response of precipitation transpire in the boreal summer, especially in India, Southeast Asia, East Asia, and Northern Africa. Whereas, it is in the western and eastern United States and western South America, southern Africa, and Southeast Asia for boreal winter. Furthermore, Jo et al. (2022) also reported that the summer monsoon season demonstrates a distinct hysteresis behavior in extreme precipitation (R30 mm) over East Asia. However, to explore more detailed information on the seasonality of hysteresis, we must consider your suggestion in our further study. However, the asymmetric change can stimulate the significant existence of hysteresis and irreversibility effect in extreme precipitation. Spatially, ~69% of the global land (average area of all the three indices) where high population density exists is expected to experience irreversible changes in extreme precipitation in response to $CO_2$ forcing. The hysteresis area is prominent over most global land monsoon regions. Typically, the unusual carbon uptake and heat by the ocean and soils over the decade to millennial timescales can control both the hysteretic and irreversible behaviors. Such widespread hysteresis and reversibility phenomena in extreme precipitation could be influenced by the complex hydrological cycle as its compound climate components have varying adjustment timescales with regard to anthropogenic GHG forcing. Kim et al. (2022) reported that the regional features of hysteresis and reversibility are determined by the rate of $CO_2$ forcing. However, the physical mechanisms for the hysteresis and reversibility of different climatic parameters and associated extremes are regionally dependent. Kug et al. (2022) reported that the large precipitation hysteresis in the tropical pacific is influenced by the hysteresis of Inter Tropical Convergence Zone (ITCZ) due to the sluggish ocean circulation adjustment linked to cross-equatorial energy exchanges between the Northern and Southern hemispheres. While Song et al. (2022) stated that such hysteresis over East Asia can be explained by the El Niño-like warming and its linkage with increased sea surface temperature in the Western-North pacific region.

Furthermore, this study further identified the hotspots for irreversible change over more than 20% of the global land. Hotspots area evolves mainly in South Asia, Southeast, and Northeast Asia, Australia, South Africa, South, and North America, and coastal regions of Antarctica which include most of the developing countries such as India, China, Bangladesh, Myanmar, Indonesia, Mozambique, Madagascar, Zambia, Chile, Peru, Ecuador, Brazil, and Uruguay as well as fewer developed countries like the United States, Canada, Australia, South Korea, and New Zealand. Boldly speaking that the global hotspots of irreversible changes in extreme precipitation mainly concentrated over the coastal regions of global land. We think the dynamically induced monsoon precipitation is more dominant than simple specific humidity change due to temperature change in this CDR experiment. It is well known that precipitation sensitivity to temperature is much weaker than that of specific humid. Thus, strong precipitation change may be attributed to the circulation change.The global land monsoon region (including most coastal regions) is one of the most impacted by extreme precipitation, perhaps associated with its abundant moisture transport from the adjacent oceans and favorable monsoonal circulation (Zhang and Zhou, 2019). Therefore, significant change in extreme precipitation is supposed to occur over strong moisture gradient regions, such as coastal areas. Kim et al. (2022) also reported a similar pattern of hotspots of irreversibility in global climate change in terms of temperature and precipitation change. However, such uneven patterns of hotspots between developing and developed land areas signify the existence of prominent regional inaptness in climate reversibility with regard to human-induced warming. The dominant presence of the irreversibile effect in developing countries signposts the persistent impact of human-induced $CO_2$ forcing, resulting in massive prospective socioeconomic damages caused by increased climate-change-related risks (Mertz et al., 2009; Cai and Lontzek, 2019).

Climate-induced risk assessment in terms of socioeconomic exposure estimation could be the key to policymaking as it links effect and adaptation. Population exposure to precipitation-related extreme events implies the speed of the social structure being affected by the hazard. Our results figure out an evident and extensive upsurge in the population exposed to extreme precipitation for all the selected SSP scenarios combined with RU and RD periods compared to the PD period. Similar findings also reported by most of the past studies using different phases of CMIP (mainly CMIP3, CMIP5, and CMIP6) that future exposure will increase compared to historical/present time (Zhang and Zhou, 2020; Liu et al., 2020; Chen and Sun, 2021; Mondal et al., 2021, 2022). Furthermore, in the scenario comparison aspects, the exposed population aggregated over global whole areas is slightly higher for all the scenario combinations with RD period than RU period. Notably, even more, an increase in the exposed population for RD combinations than RU is found when it averaged over only the hotspots area of irreversibility. Such strong differences could arise due to the presence of widespread climate change hysteresis over the hotspot areas. This feature of exposure change is certainly different from the past estimation of socioeconomic exposure based on global climate models and emission scenarios (mainly CMIP3, CMIP5, and CMIP6). Most of the previous studies stated a substantial increase in socioeconomic exposure under the future scenario designed with high GHG emission, whereas our findings suggest larger exposure in RD ($CO_2$ reduction) period. It may happen due to persistent characteristics of global warming, even if atmospheric $CO_2$ is reduced, the induced warming would not decrease at the same speed. In relative terms, exposure is projected even more higher over areas in central-, and southern-Africa, as well as southern-, and eastern-Asia. The spatial pattern of exposure due to extreme precipitation is largely similar to previous studies based on global climate models and emission scenarios (mainly from CMIP5, and CMIP6) (Zhang and Zhou, 2020; Liu et al., 2020). So, it can be boldly underlined that the people in Africa and Asia regions are highly vulnerable to future precipitation-related extremes. The area-averaged estimation and spatial distribution signify the leading exposure under the SSP3 pathway combined with both RU (SSP3-RU) and RD (SSP3-RD). Usually, the SSP3 pathway is known to pose high social vulnerability where the global population growth is much higher and intended to continue toward the next several decades (Fig. S6). The growing population, high inequality, uncontrolled emission, slow technological upgradation in the energy sector, and low investment in human resource development are some basic features of SSP3 leading to high mitigation and adaptation challenges (O'Neill et al., 2014). This study further explored the relative contribution of different causal factors of the change in exposure (climate change effect, population change effect, and

climate-population combined change effect) to provide a window of informing policy response to reduce the exposed population to extreme precipitation. The analysis signifies that the population change effect is the prime contributor to exposure change aggregated over the global total land area. It is the signpost of rapid population growth globally without proper control measures. This finding is consistent with most of the previous studies (Zhang and Zhou, 2020; Liu et al., 2020; Chen and Sun, 2021). In contrast, the climate change effect is the pivotal contributor to the exposure change aggregated over only the hotspot area. This indicates that the population exposure over the hotspots region is largely due to increased extreme precipitation frequency. Notably, the role of climate change effect is prospective to escalate over time for both the global and hotspots aspects. However, such a contrasting role indicates a strong regional variation; exposure in a different region is influenced by different factors. Similar regional variation in the relative importance of different influential factors in exposure change was also reported by Chen & Sun (2021).

This research work discourses some limitations associated with climate variable projections and population modeling approaches, which might affect the trustworthiness of our results. In this study, the climatic variable precipitation produced by the climate models yields differences with regard to actual features of the world's climate. The CESM is a coarse model and thus does not simulate severe storms very realistically. It has precipitation bias. Therefore, our precipitation hysteresis map as well as hotspots of irreversibility may be affected by this bias. It might be tough to reproduce climate parameters securing consistency with the real climatic condition. However, the use of ensembles of multiple simulations is widely acknowledged and evaluated by scientific communities with satisfactory outcomes. Further, the response to $CO_2$ forcing is calculated over the average of 140 years by comparing the difference between RU and RD. The use of mean calculated over such long time period may weakened the signal of $CO_2$ effect. However, even if we pick a specific time slice and compared them, we may lose some information in different responses in a different time frame (Fig. S8). Moreover, the population projection method does not consider the change in individual countries' policy interventions related to population-growth control. Moreover, as the population projections for distant-future (i.e. after 2 100) is not available, we did not maintain consistent timescales for both precipitation and population.

However, this study offers some pivotal insights with a scientific basis to formulate effective policy interventions. The asymmetric response of extreme precipitation and associated population exposure signify that only $CO_2$ reduction would not be enough to cope with future climate change-related risks, rather effective adaptation policies should essentially be initiated to manage anticipated risk. Further, the annual exposure caused by extreme precipitation may not be reduced/avoided only if $CO_2$ forcing is set back to its initial state (Fig. S7). However, the population growth control policy is the key aspect to reducing global population exposure to extreme precipitation, while policymaking focusing on climate change mitigation in some regions is crucial. Effective policymaking considering population control and climate change mitigation through $CO_2$ cuts can reduce the number of people affected by extreme precipitation. Regionally, regarding exposure reduction, more attention should be paid to South Africa and Asia regions, especially in controlling the growing population. So, it is an urgent need to develop and accomplish more advanced and diverse adaptation and mitigation measures to fortify socioeconomic structures to cope with extreme precipitation.

## Authors contributions

Soon-Il An, and Seung-Ki Min conceived the research concept as well as incorporated innovative ideas. Sanjit Kumar Mondal mainly contributed to this research by carrying out major analyses and drafting the manuscript. Soong-Ki Kim, Jongsoo Shin, and Seungmok Paik computed the precipitation-related extreme index at the global aspects. Nari Im and Liu downloaded and processed population data. Finally, all authors reviewed and edited the manuscript.

## Declaration of competing interest

The authors declare that they have no known competing financial interests or personal relationships that could have appeared to influence the work reported in this paper.

## Data availability

Data will be made available on request.

## Acknowledgments and data

Our research work was jointly supported by the National Research Foundation of Korea (NRF), Korea Government (MSIT) (NRF-2018R1A5A1024958), and Yonsei Signature research Cluster Program of 2021 (2021-22-0003). All the authors express their gratitude to those institutes/organizations provided data in this study. Model simulation and data transfer were supported by the National Supercomputing Center with supercomputing resources including technical support (KSC-2021-CHA-0030), the National Center for Meteorological Supercomputer of the Korea Meteorological Administration (KMA), and by the Korea Research Environment Open NETwork (KREONET), respectively.

## Appendix A. Supplementary data

Supplementary data to this article can be found online at https://doi.org/10.1016/j.wace.2023.100561.

## References

Alexander, L.V., Zhang, X., Peterson, T.C., Caesar, J., Gleason, B., Klein Tank, A.M.G., et al., 2006. Global observed changes in daily climate extremes of temperature and precipitation. J. Geophys. Res. 111 (D5), D05109 https://doi.org/10.1029/2005JD006290.

An, S., Shin, J., Yeh, S., Son, S., Kug, J., Min, S., Kim, H., 2021a. Global cooling hiatus driven by an AMOC overshoot in a carbon dioxide removal scenario. Earth's Future 9 (7). https://doi.org/10.1029/2021EF002165.

An, S., Kim, H., Kim, S., 2021b. Rate-dependent hysteresis of the atlantic meridional overturning circulation system and its asymmetric loop. Geophys. Res. Lett. 48 (1) https://doi.org/10.1029/2020GL090132.

An, S.-I., Park, S.-E., Shin, J., Yang, Y.-M., Yeh, S.-W., Son, S.-W., Kug, J.-S., 2022. General circulation and global heat transport in a quadrupling CO2 pulse experiment. Sci. Rep. 12 (1), 11569 https://doi.org/10.1038/s41598-022-15905-0.

Armstrong McKay, D.I., Staal, A., Abrams, J.F., Winkelmann, R., Sakschewski, B., Loriani, S., et al., 2022. Exceeding 1.5°C global warming could trigger multiple climate tipping points. Science 377 (6611). https://doi.org/10.1126/science.abn7950.

Ayugi, B., Jiang, Z., Iyakaremye, V., Ngoma, H., Babaousmail, H., Onyutha, C., et al., 2022. East African population exposure to precipitation extremes under 1.5 °C and 2.0 °C warming levels based on CMIP6 models. Environ. Res. Lett. 17 (4), 044051 https://doi.org/10.1088/1748-9326/ac5d9d.

Boucher, O., Halloran, P.R., Burke, E.J., Doutriaux-Boucher, M., Jones, C.D., Lowe, J., et al., 2012. Reversibility in an Earth System model in response to CO 2 concentration changes. Environ. Res. Lett. 7 (2), 024013 https://doi.org/10.1088/1748-9326/7/2/024013.

Cai, Y., Lontzek, T.S., 2019. The social cost of carbon with economic and climate risks. J. Polit. Econ. 127 (6), 2684–2734. https://doi.org/10.1086/701890.

Caldeira, K., Myhrvold, N.P., 2013. Projections of the pace of warming following an abrupt increase in atmospheric carbon dioxide concentration. Environ. Res. Lett. 8 (3), 034039 https://doi.org/10.1088/1748-9326/8/3/034039.

Cao, L., Bala, G., Caldeira, K., 2011. Why is there a short-term increase in global precipitation in response to diminished CO 2 forcing? Geophys. Res. Lett. 38 (6) https://doi.org/10.1029/2011GL046713 n/a-n/a.

Carleton, T.A., Hsiang, S.M., 2016. Social and economic impacts of climate. Science 353 (6304). https://doi.org/10.1126/science.aad9837.

Ceola, S., Laio, F., Montanari, A., 2014. Satellite nighttime lights reveal increasing human exposure to floods worldwide. Geophys. Res. Lett. 41 (20), 7184–7190. https://doi.org/10.1002/2014GL061859.

Chadwick, R., Wu, P., Good, P., Andrews, T., 2013. Asymmetries in tropical rainfall and circulation patterns in idealised CO2 removal experiments. Clim. Dynam. 40 (1–2), 295–316. https://doi.org/10.1007/s00382-012-1287-2.

Chen, H., Sun, J., 2021. Significant increase of the global population exposure to increased precipitation extremes in the future. Earth's Future 9 (9). https://doi.org/10.1029/2020EF001941.
Chen, H., Sun, J., Li, H., 2020. Increased population exposure to precipitation extremes under future warmer climates. Environ. Res. Lett. 15 (3), 034048 https://doi.org/10.1088/1748-9326/ab751f.
Donat, M.G., Lowry, A.L., Alexander, L.V., O'Gorman, P.A., Maher, N., 2016. More extreme precipitation in the world's dry and wet regions. Nat. Clim. Change 6, 508–513. https://doi.org/10.1038/nclimate2941.
Field, C.B., Barros, V., Stocker, T.F., Dahe, Q. (Eds.), 2012. Managing the Risks of Extreme Events and Disasters to Advance Climate Change Adaptation. Cambridge University Press. https://doi.org/10.1017/CBO9781139177245.
Fischer, T., Menz, C., Su, B., Scholten, T., 2013. Simulated and projected climate extremes in the Zhujiang River Basin, South China, using the regional climate model COSMO-CLM. Int. J. Climatol. 33, 2988–3001. https://doi.org/10.1002/joc.3643.
Gao, J., 2020. Global 1-km Downscaled Population Base Year and Projection Grids Based on the Shared Socioeconomic Pathways, Revision 01. Palisades. NASA Socioeconomic Data and Applications Center (SEDAC), New York. https://doi.org/10.7927/q7z9-9r69.
Garbe, J., Albrecht, T., Levermann, A., Donges, J.F., Winkelmann, R., 2020. The hysteresis of the antarctic ice sheet. Nature 585 (7826), 538–544. https://doi.org/10.1038/s41586-020-2727-5.
Hawkins, E., Smith, R.S., Allison, L.C., Gregory, J.M., Woollings, T.J., Pohlmann, H., de Cuevas, B., 2011. Bistability of the Atlantic overturning circulation in a global climate model and links to ocean freshwater transport. Geophys. Res. Lett. 38 (10) https://doi.org/10.1029/2011GL047208 n/a-n/a.
Hunke, E.C., Lipscomb, W.H., 2010. CICE: The Los Alamos sea ice model documentation and software user's manual, version 4.1. LA-CC-06-012. Alamos National Laboratory, Los, p. 76pp.
Hurrell, J.W., Holland, M.M., Gent, P.R., Ghan, S., Kay, J.E., Kushner, P.J., et al., 2013. The community earth system model: a framework for collaborative research. Bull. Am. Meteorol. Soc. 94 (9), 1339–1360. https://doi.org/10.1175/BAMS-D-12-00121.1.
IPCC, 2013. In: Stocker, T.F., Qin, D., Plattner, G.-K., Tignor, M., Allen, S.K., Boschung, J., Nauels, A., Xia, Y., Bex, V., Midgley, P.M. (Eds.), Climate Change 2013: the Physical Science Basis. Contribution of Working Group I to the Fifth Assessment Report of the Intergovernmental Panel on Climate Change. Cambridge University Press, Cambridge, United Kingdom and New York, NY, USA, p. 1535.
IPCC, 2018. Global Warming of 1.5°C. An IPCC Special Report on the impacts of global warming of 1.5°C above pre-industrial levels and related global greenhouse gas emission pathways. In: Zhai, V.P., Pörtner, H.-O., Roberts, D., Skea, J., Shukla, P.R., Pirani, A., Moufouma-Okia, W., Péan, C., Pidcock, R., Connors, S., Matthews, J.B.R., Chen, Y., Zhou, X., Gomis, M.I., Lonnoy, E., Maycock, T., Tignor, M., Waterfield, T. (Eds.), The Context of Strengthening the Global Response to the Threat of Climate Change, Sustainable Development, and Efforts to Eradicate Poverty [Masson-Delmotte. World Meteorological Organization, Geneva, Switzerland.
IPCC, 2021. Summary for policymakers. In: Zhai, P., Pirani, A., Connors, S.L., Péan, C., Berger, S., Caud, N., Chen, Y., Goldfarb, L., Gomis, M.I., Huang, M., Leitzell, K., Lonnoy, E., Matthews, J.B.R., Maycock, T.K., Waterfield, T., Yelekçi, O., Yu, R., Zhou, B. (Eds.), Climate Change 2021: the Physical Science Basis. Contribution of Working Group I to the Sixth Assessment Report of the Intergovernmental Panel on Climate Change [Masson-Delmotte, V. Cambridge University Press (in press).
Jo, S., Seong, M., Min, S., Kug, J., Yeh, S., An, S., et al., 2022. Hysteresis behaviors in East Asian extreme precipitation frequency to CO 2 pathway. Geophys. Res. Lett. 49 (18) https://doi.org/10.1029/2022GL099814.
Jones, B., O'Neill, B.C., McDaniel, L., McGinnis, S., Mearns, L.O., Tebaldi, C., 2015. Future population exposure to US heat extremes. Nat. Clim. Change 5 (7), 652–655. https://doi.org/10.1038/nclimate2631.
Keller, D.P., Lenton, A., Scott, V., Vaughan, N.E., Bauer, N., Ji, D., et al., 2018. The carbon dioxide removal model intercomparison Project (CDRMIP): rationale and experimental protocol for CMIP6. Geosci. Model Dev. (GMD) 11 (3), 1133–1160. https://doi.org/10.5194/gmd-11-1133-2018.
Kim, S.K., Shin, J., An, S. Il, Kim, H.J., Im, N., Xie, S.P., et al., 2022. Widespread irreversible changes in surface temperature and precipitation in response to CO2 forcing. Nat. Clim. Change 12 (9), 834–840. https://doi.org/10.1038/s41558-022-01452-z.
Kug, J.S., Oh, J.H., An, S. Il, Yeh, S.W., Min, S.K., Son, S.W., et al., 2022. Hysteresis of the intertropical convergence zone to CO2 forcing. Nat. Clim. Change 12 (1), 47–53. https://doi.org/10.1038/s41558-021-01211-6.
Lawrence, D.M., Oleson, K.W., Flanner, M.G., Thornton, P.E., Swenson, S.C., Lawrence, P.J., et al., 2011. Parameterization improvements and functional and structural advances in version 4 of the community land model. J. Adv. Model. Earth Syst. 3 (3), M03001 https://doi.org/10.1029/2011MS000045.
Liu, Y., Chen, J., Pan, T., Liu, Y., Zhang, Y., Ge, Q., et al., 2020. Global socioeconomic risk of precipitation extremes under climate change. Earth's Future 8 (9). https://doi.org/10.1029/2019EF001331.
Lu, J., Cai, M., 2010. Quantifying contributions to polar warming amplification in an idealized coupled general circulation model. Clim. Dynam. 34 (5), 669–687. https://doi.org/10.1007/s00382-009-0673-x.
MacDougall, A.H., 2013. Reversing climate warming by artificial atmospheric carbon-dioxide removal: can a Holocene-like climate be restored? Geophys. Res. Lett. 40 (20), 5480–5485. https://doi.org/10.1002/2013GL057467.
Mertz, O., Halsnæs, K., Olesen, J.E., Rasmussen, K., 2009. Adaptation to climate change in developing countries. Environ. Manag. 43 (5), 743–752. https://doi.org/10.1007/s00267-008-9259-3.
Mondal, S.K., Huang, J., Wang, Y., Su, B., Zhai, J., Tao, H., et al., 2021. Doubling of the population exposed to drought over South Asia: CMIP6 multi-model-based analysis. Sci. Total Environ. 771, 145186 https://doi.org/10.1016/j.scitotenv.2021.145186.
Mondal, S.K., Wang, Y., Zhai, J., Su, B., Jiang, S., Huang, J., et al., 2022. Projected urban exposure to extreme precipitation over South Asia. Sci. Total Environ. 822, 153664 https://doi.org/10.1016/j.scitotenv.2022.153664.
Neale, R.B., Gettelman, A., Park, S., Conley, A.J., Kinnison, D., Marsh, D., et al., 2010. Description of the NCAR Community Atmosphere Model (CAM 5.0). Tech. Note NCAR/TN- 486+STR, Natl. Cent. for Atmos.
Oh, H., An, S., Shin, J., Yeh, S., Min, S., Son, S., Kug, J., 2022. Contrasting hysteresis behaviors of northern Hemisphere land monsoon precipitation to CO 2 pathways. Earth's Future 10 (6). https://doi.org/10.1029/2021EF002623.
Ohba, M., Tsutsui, J., Nohara, D., 2014. Statistical parameterization expressing ENSO variability and reversibility in response to CO2 concentration changes. J. Clim. 27 (1), 398–410. https://doi.org/10.1175/JCLI-D-13-00279.1.
O'Neill, B.C., Kriegler, E., Riahi, K., Ebi, K.L., Hallegatte, S., Carter, T.R., Mathur, R., van Vuuren, D.P., 2014. A new scenario framework for climate change research: the concept of shared socioeconomic pathways. Clim. Change 122, 387–400. https://doi.org/10.1007/s10584-013-0905-2.
Paik, S., Min, S., Zhang, X., Donat, M.G., King, A.D., Sun, Q., 2020. Determining the anthropogenic greenhouse gas contribution to the observed intensification of extreme precipitation. Geophys. Res. Lett. 47 (12) https://doi.org/10.1029/2019GL086875.
Peng, D., Zhou, T., Zhang, L., Zhang, W., Chen, X., 2020. Observationally constrained projection of the reduced intensification of extreme climate events in Central Asia from 0.5 °C less global warming. Clim. Dynam. 54 (1–2), 543–560. https://doi.org/10.1007/s00382-019-05014-6.
Pinskwar, I., Chorynski, A., Graczyk, D., Kundzewicz, Z.W., 2019. Observed changes in extreme precipitation in Poland: 1991-2015 versus 1961-1990. Theor. Appl. Climatol. 135 (1–2), 773–787.
Pollard, D., DeConto, R.M., 2005. Hysteresis in cenozoic antarctic ice-sheet variations. Global Planet. Change 45 (1–3), 9–21. https://doi.org/10.1016/j.gloplacha.2004.09.011.
Rahmstorf, S., Crucifix, M., Ganopolski, A., Goosse, H., Kamenkovich, I., Knutti, R., et al., 2005. Thermohaline circulation hysteresis: a model intercomparison. Geophys. Res. Lett. 32 (23), L23605 https://doi.org/10.1029/2005GL023655.
Shen, L., Wen, J., Zhang, Y., Ullah, S., Cheng, J., Meng, X., 2022. Changes in population exposure to extreme precipitation in the Yangtze River Delta, China. Climate Services 27, 100317. https://doi.org/10.1016/j.cliser.2022.100317.
Shi, X., Chen, J., Gu, L., Xu, C.-Y., Chen, H., Zhang, L., 2021. Impacts and socioeconomic exposures of global extreme precipitation events in 1.5 and 2.0 °C warmer climates. Sci. Total Environ. 766, 142665 https://doi.org/10.1016/j.scitotenv.2020.142665.
Skific, N., Francis, J.A., Cassano, J.J., 2009. Attribution of projected changes in atmospheric moisture transport in the arctic: a self-organizing map perspective. J. Clim. 22 (15), 4135–4153. https://doi.org/10.1175/2009JCLI2645.1.
Smith, R., Jones, P., Briegleb, B.P., Bryan, F.O., Danabasoglu, G., Dennis, J., et al., 2010. The Parallel Ocean Program (POP) reference manual: Ocean component of the Community Climate System Model (CCSM) and community earth system model (CESM). LAUR-01853, pp. 1–140.
Song, S.-Y., Yeh, S.-W., An, S.-I., Kug, J.-S., Min, S.-K., Son, S.-W., Shin, J., 2022. Asymmetrical response of summer rainfall in East Asia to CO2 forcing. Sci. Bull. 67 (2), 213–222. https://doi.org/10.1016/j.scib.2021.08.013.
Trenberth, K.E., Jones, P.D., Ambenje, P., Bojariu, R., Easterling, D., Klein Tank, A., Parker, D., Rahimzadeh, F., Renwick, J.A., Rusticucci, M., Soden, B., Zhai, P., 2007. Observations: surface and atmospheric climate change. In: Solomon, S., Qin, D., Manning, M., Chen, Z., Marquis, M., Averyt, K.B., Tignor, M., Miller, H.L. (Eds.), Climate Change 2007: the Physical Science Basis. Contribution of Working Group I to the Fourth Assessment Report of the Intergovernmental Panel on Climate Change. Cambridge University Press, Cambridge, United Kingdom and New York, NY, USA.
Trenberth, K., 2011. Changes in precipitation with climate change. Clim. Res. 47, 123–138. https://doi.org/10.3354/cr00953.
United Nations International Strategy for Disaster Reduction (UNISDR), 2017. Terminology. https://www.unisdr.org/we/inform/terminology#letter-e/.
Westra, S., Alexander, L.V., Zwiers, F.W., 2013. Global increasing trends in annual maximum daily precipitation. J. Clim. 26, 3904–3918. https://doi.org/10.1175/JCLI-D-12-00502.1.
Wu, P., Wood, R., Ridley, J., Lowe, J., 2010. Temporary acceleration of the hydrological cycle in response to a CO 2 rampdown. Geophys. Res. Lett. 37 (12) https://doi.org/10.1029/2010GL043730 n/a-n/a.
Yeh, S.-W., Song, S.-Y., Allan, R.P., An, S.-I., Shin, J., 2021. Contrasting response of hydrological cycle over land and ocean to a changing CO2 pathway. NPJ Climate Atmosphere Sci. 4 (1), 53. https://doi.org/10.1038/s41612-021-00206-6.
Zhan, M., Zhai, J., Sun, H., Li, X., Xia, L., 2019. Observed exposure of population and gross domestic product to extreme precipitation events in the poyang lake basin, China. Atmosphere 10 (12), 817. https://doi.org/10.3390/atmos10120817.
Zhang, W., Zhou, T., 2019. Significant increases in extreme precipitation and the associations with global warming over the global land monsoon regions. J. Clim. 32 (24), 8465–8488. https://doi.org/10.1175/JCLI-D-18-0662.1.
Zhang, W., Zhou, T., 2020. Increasing impacts from extreme precipitation on population over China with global warming. Sci. Bull. 65 (3), 243–252. https://doi.org/10.1016/j.scib.2019.12.002.

Zhang, W., Zhou, T., Zou, L., Zhang, L., Chen, X., 2018. Reduced exposure to extreme precipitation from 0.5 °C less warming in global land monsoon regions. Nat. Commun. 9 (1), 3153. https://doi.org/10.1038/s41467-018-05633-3.
Zhao, J.-T., Su, B.-D., Mondal, S.K., Wang, Y.-J., Tao, H., Jiang, T., 2021. Population exposure to precipitation extremes in the Indus River Basin at 1.5 °C, 2.0 °C and 3.0 °C warming levels. Adv. Clim. Change Res. 12 (2), 199–209. https://doi.org/10.1016/j.accre.2021.03.005.
Zickfeld, K., MacDougall, A.H., Matthews, H.D., 2016. On the proportionality between global temperature change and cumulative CO 2 emissions during periods of net negative CO 2 emissions. Environ. Res. Lett. 11 (5), 055006 https://doi.org/10.1088/1748-9326/11/5/055006.